Materialia 8 (2019) 100461

Contents lists available at ScienceDirect

Materialia

journal homepage: www.elsevier.com/locate/mtla

Full Length Article

Tuning mechanical properties of electrospun piezoelectric nanofibers by heat treatment

Tu-Ngoc Lam[a,b], Chun-Chieh Wang[c,*], Wen-Ching Ko[a,d], Jyh-Ming Wu[e], Sz-Nian Lai[e], Wei-Tsung Chuang[c], Chun-Jen Su[c], Chia-Yin Ma[a], Mao-Yuan Luo[a], Ying-Jhih Wang[a], E-Wen Huang[a,*]

[a] Department of Materials Science and Engineering, National Chiao Tung University, 1001 University Road, Hsinchu 30010, Taiwan (R.O.C.)
[b] Department of Physics, College of Education, Can Tho University, Can Tho City, Vietnam
[c] National Synchrotron Radiation Research Center, Hsinchu 30076, Taiwan (R.O.C.)
[d] Institute of Applied Mechanics, National Taiwan University, 1, Sec. 4, Roosevelt Road, Taipei 106, Taiwan (R.O.C.)
[e] Department of Materials Science and Engineering, National Tsing Hua University, Hsinchu 30013, Taiwan (R.O.C.)

ARTICLE INFO

Keywords:
Electrospun nanofibers
Piezoelectricity
Deformation
Small and wide angle X-ray scattering
Transmission X-ray microscopy

ABSTRACT

We report an annealing method which significantly enhances the piezoelectric performance by simultaneously tuning morphology and crystalline phase of electrospun P(VDF-TrFE) nanofibers. Annealing process-induced transformation, from α to β crystalline phase at lattice scale, also changes fiber morphology at micrometer scale. The underlying differences between as-spun and annealed P(VDF-TrFE) nanofibers for their stretch-hold deformation were examined via *in-situ* synchrotron for both small and wide angle X-ray scattering (SAXS and WAXS). Transmission X-ray microscopy (TXM) characterization reveals the underneath fiber orientation subjected to different levels of deformation. Multi-length scale microstructural evolution demonstrates distinct deformation behaviors of the as-spun and annealed nanofibers during uniaxial tensile loading. The findings can be applied for multi-scale structure modulation for the design of future piezoelectric devices.

1. Introduction

Poly[(vinylidene fluoride)-co-trifluoroethylene] [P(VDF-TrFE)], one of the co-polymers of poly(vinylidene fluoride) (PVDF), has recently attracted increasing attention in various application fields of wearable electronics, flexible sensors, and energy harvesting due to its superior properties such as lightweight, tunable, stable, biocompatible, stretchable, and flexible [1–11]. P(VDF-TrFE) material has been known to possess good piezoelectric performance which may be tailored through different processing techniques. Among the most popular polymer fabrication technologies, electrospinning has emerged as an effective and promising method to produce high quality nanofibrous membranes composed of ultrafine nanofibers which have better energy conversion efficiency [2,5,6,8,12]. Moreover, electrospinning technique enables the formation of highly aligned electrical dipoles as well high amount of polar β crystalline phase which is directly proportional to the piezoelectricity [6–8,13].

P(VDF-TrFE) is a semi-crystalline polymer owning polymorphic crystalline phases [14–17] whose individual crystal structure is able to be tuned and converted each other via fabrication process or different treatment methods. Among polymorphic phases, the polar β crystalline phase discloses the best piezoelectric response with highly oriented dipole moments. It has been reported by various research studies that the more the β crystalline phase, the better the piezoelectric performance [5,14,18]. Thus, great efforts have been made to solve one of the most appealing questions, that is how to transform or create the entire β crystalline phase P(VDF-TrFE) for the best piezoelectric characteristics [13,14]. Besides good piezoelectricity, strong mechanical properties of high strength, high modulus, ductility, and fracture toughness are vital requisites for feasible and potential applicability of P(VDF-TrFE) membranes in practical devices [2,14]. Different kinds of methods have been conducted to convert the dominant crystalline structure from α to β crystalline phase as well as to improve the mechanical behavior of P(VDF-TrFE) [16,19–22]. Uniaxial stretching α crystalline phase is one of the most prevalent approaches causing α to β transformation. In addition, many studies have demonstrated tailored microstructure and piezoelectric performances of P(VDF-TrFE) films subjected to different annealing temperatures within the range between Curie temperature ($T_c \sim 118$ °C) and melting temperature ($T_m \sim 144$ °C) [11,13,23–25]. Specifically, annealing P(VDF-TrFE) at or slightly above the T_c (around 120 °C) for

* Corresponding authors.
E-mail addresses: wang.jay@nsrrc.org.tw (C.-C. Wang), ewenhuang@nctu.edu.tw (E.-W. Huang).

https://doi.org/10.1016/j.mtla.2019.100461
Received 22 April 2019; Accepted 29 August 2019
Available online 31 August 2019
2589-1529/© 2019 Acta Materialia Inc. Published by Elsevier Ltd. This is an open access article under the CC BY license.
(http://creativecommons.org/licenses/by/4.0/)

2 h was found to induce maximum polar β crystalline phase with high remanent polarization and superior surface morphology [11,23,24].

Although the phase transformation and mechanical properties of P(VDF-TrFE) have been investigated, the coupling between crystal structure and morphology during stretching deformation of electrospun P(VDF-TrFE) nanofibers is not conclusive yet [13,26–29]. In this work, we extended from our earlier findings to examine the deformation mechanisms at the multi-length scale behaviors of nanofibers alignment under uniaxial straining through mechanical, structural and morphological characterizations for as-spun and annealed P(VDF-TrFE) nanofibers fabricated by electrospinning. The influence of annealing process on the structural and morphological responses of P(VDF-TrFE) nanofibers was explored by employing *in-situ* concomitant synchrotron small and wide angle X-ray scattering (SAXS and WAXS) techniques accompanied with scanning electron microscopy (SEM) under the stretch-hold deformation.

2. Experiment

2.1. Sample preparation

The mixture of Dimethylacetamide (DMC) and Methyl Ethyl Ketone (MEK) with the weight ratio of 2:3 was used as a cosolvent. The electrospinning solution with the optimal concentration of 12% was prepared by dissolving P(VDF-TrFE) (75/25 mol%) (Kureha Trading Co., Ltd) in the cosolvent and stirred uniformly at 60° until a transparent solution was obtained. The as-spun membrane was annealed at 120 °C for 2 h and subsequently furnace cooled to become the annealed P(VDF-TrFE) sample, following the optimized annealing condition in achieving high efficiency of polar β crystalline phase.

2.2. Mechanical test

P(VDF-TrFE) membrane was cut into dumbbell-shaped specimen with an overall length of 50 mm, a gage length and width of 10 mm and 3 mm, respectively, a distance between shoulders of 24 mm. The uniaxial tensile strength test was recorded at a strain rate of 0.05 mm/s and a holding time of 10 s between successive strains to record the *in-situ* concurrent SAXS and WAXS patterns.

2.3. Piezoelectric test

The output short-circuit current and open-circuit voltage of the PENG (Piezo-electric Nanogenerator) were measured using a low-noise current preamplifier (Stanford Research System Model SR570), a low-noise voltage preamplifier (Stanford Research System Model SR560), and a Keithley 6514 programmable electrometer. The motion and strain were controlled by the linear motor system (Linmot Talk 5.1 motor system) as the mechanical force source with a displacement of 1 cm and a frequency of 1 Hz.

2.4. Transmission X-ray microscopy

Transmission X-ray microscopy is a non-destructive image microscopy technique, which allows internal microstructure analysis of fiber orientation in fibrous materials. TXM was carried out at beamline (BL) 01B1, National Synchrotron Radiation Research Center (NSRRC) in Taiwan with the wavelength of 1.54 Å (8 keV) and spatial resolution of 60 nm [30–32].

2.5. Synchrotron small and wide angle X-ray scattering

The non-destructive X-ray scattering techniques were implemented with the wavelength of 1.24 Å (10 keV) at BL 23A, NSRRC, Taiwan. The SAXS [33] and WAXS [18] scattering patterns were collected from a two-dimensional (2D) detector and calibrated by background subtraction. Long period was calculated by determining the peak positions extracted from 2D SAXS.

3. Results and discussion

3.1. The role of annealing treatment

Understanding the effect of annealing process on the structural and mechanical characterizations of electrospun P(VDF-TrFE) nanofibers is of great crucial for their potential applications. The impact of annealing on surface morphology and structure changes of electrospun P(VDF-TrFE) membrane was investigated by SEM together with one-dimensional (1D) WAXS profiles. Fig. 1(a) and (b) shows the top-view SEM images before and after annealing P(VDF-TrFE). The random arrangement of homogeneous nanofibers was denser in the annealed than in the as-spun P(VDF-TrFE) specimen. Based on the average diameter quantification analysis in Fig. 1(c), annealing process leads to larger nanofiber diameter of 353 nm compared to that of 283 nm in the as-spun P(VDF-TrFE), may be ascribed to the nucleation of cavities or microvoids as well the aggregation of rearranged molecular chains. Furthermore, it can be observed in the cross-section SEM images that annealing treatment thickens nanofiber distribution density and decreases the total membrane thickness from 91 μm to 57 μm, as shown in Fig. S1 of the supplementary. In Fig. 1(d), the 1D WAXS patterns of as-spun P(VDF-TrFE) presented four distinct diffraction peaks which were assigned to the (110)α, (200)β, (020)β and (111)β, suggesting the α crystalline phase in the as-spun P(VDF-TrFE) membrane. Annealing P(VDF-TrFE) yields an expected disappearance of the (110)α as well as a remarkable increase in the intensity of the three sharp β diffraction patterns, implying a salient transition from α to β crystalline phase induced by annealing process. It is believed that the more the β crystalline phase is, the greater the piezoelectric and mechanical properties are [3,13,34,35]. We did achieve more pronounced piezoelectric responses in which the short-circuit current of annealed P(VDF-TrFE) was ten times greater than that of as-spun sample of 0.2 nA and the open-circuit voltage increased from 150 mV to 200 mV in the annealed P(VDF-TrFE) nanofibers, shown in Fig. 1(e) and (f). The piezoelectric output signals performed a periodical repeatability and good reliability under bending and releasing the P(VDF-TrFE) samples. Annealing treatment significantly enhances the degree of β crystalline phase and thus improves the piezoelectric response.

The underlying mechanisms involved in the annealing effect on morphological and microstructural changes can be assigned to a better and denser reconstruction of nanofibers in which the tie chains between stacked lamellar crystals tend to closely and tightly pack together with strong intermolecular bonding forces to form the more stable and compact β crystalline phase, associated with a drastic decrease of cavities, microvoids, impurities, and defects between lamella stacks. A considerable decline of the amorphous crystalline to form a more perfect and stable crystalline structure with the minimum surface free energy is another explanation for decreasing the membrane thickness under annealing effect. It can be suggested that annealing treatment is an effective and economic method to greatly enhance the expected β crystalline phase and piezoelectricity for promising applications in wearable electronics.

3.2. Deformation mechanism of as-spun P(VDF-TrFE)

We first examined the mechanical behavior associated with structural evolution of as-spun P(VDF-TrFE) membrane to identify the predominant deformation mechanism during straining. Fig. 2 describes the *in-situ* uniaxial tensile loading coupled with 2D SAXS and WAXS, together with SEM images for the as-spun P(VDF-TrFE) membrane. The structural changes were presented at the strain of 45%, 150%, and

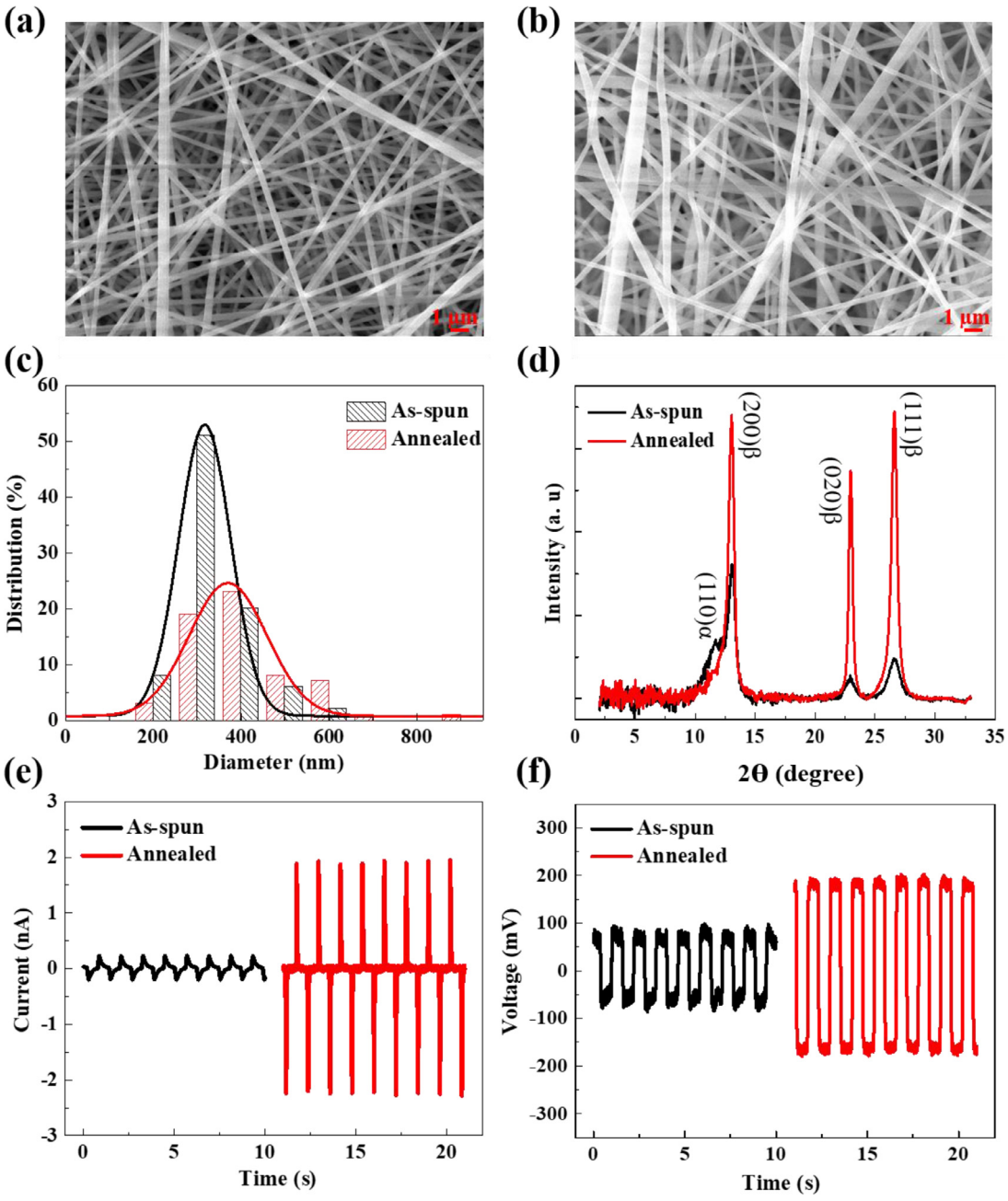

Fig. 1. Top-view SEM images (a) before and (b) after annealing electrospun P(VDF-TrFE) nanofibers. (c) Fiber distribution in the as-spun and annealed P(VDF-TrFE). (d) 1D WAXS patterns of the as-spun and annealed P(VDF-TrFE) samples. (e) The short-circuit current and (f) open-circuit voltage at the frequency 1 Hz of the as-spun and annealed P(VDF-TrFE).

285%. The holding time of 10 s in the engineering stress–strain (S–S) curve was observed as the vertical drop during the stretch-hold response. An inconspicuous yield point was obtained with the yield strength was estimated around 2.5 MPa. The striking point was a great elongation of the as-spun membrane which can be extensively stretched as long as 327%. Such an outstanding ductility macroscopic behavior of the as-spun P(VDF-TrFE) was illustrated by deformation images in Fig. 2(a)–(c) while the surface alignment of electrospun nanofibers under stretching was taken by SEM images in Fig. 2(d)–(f). TXM images of underneath fiber orientation were provided in the inset of Fig. 2(d)–(f). The S-S response in Fig. 2(g) can be divided into three distinct elastic-plastic deformation stages, namely, first stage (I) in the yielding region of 45% strain, second stage (II) after yielding (60–200% strain), and third stage (III) (200–327% strain). The dominant deformation mechanisms coupled with the underlying structure evolution in each stage under tensile loading were clarified. Before stretching, SEM image displays a randomly disorder orientation of curvy nanofibers. Under straining, P(VDF-TrFE) nanofibers gradually align towards the tensile axis, which experiences specific stages including straightening, stretching, sliding, and orderly orientation along the tensile direction. Fig. 2(d) depicts the rotation, straightening, and stretching of nanofibers during this stage of deformation. The 2D SAXS in Fig. 2(h) discloses uniformly isotropic circular ring, confirming the random distribution of α crystalline phase. The corresponding WAXS in Fig. 2(k) exhibits isotropic diffraction patterns indexed as (110)α, (200)β, (020)β and (111)β of the α crystalline phase P(VDF-TrFE). After yielding in the region II, we can observe a concurrent stretching, sliding, and aligning of nanofibers in Fig. 2(e). Such deformation behaviors not only facilitate further fiber

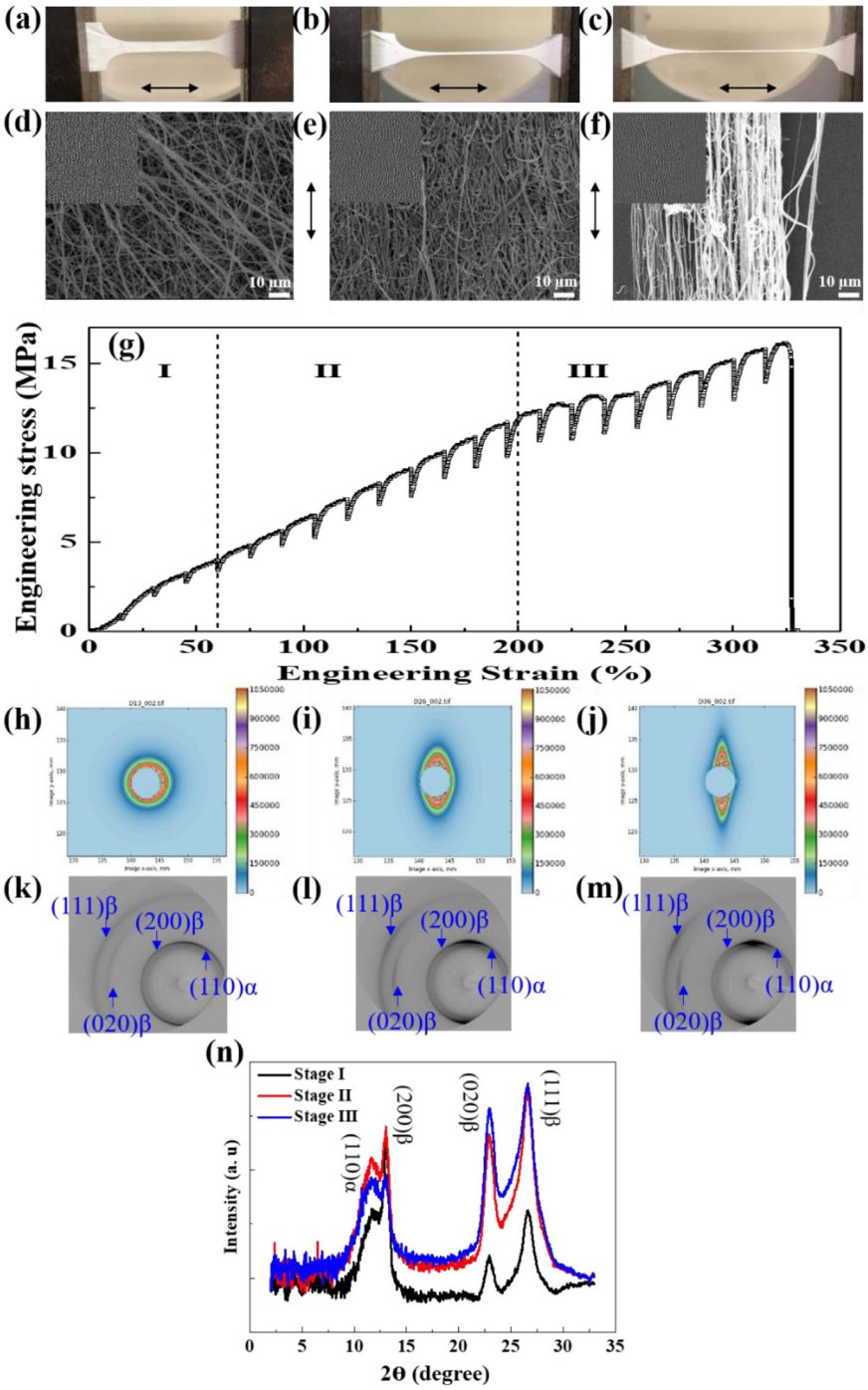

Fig. 2. (a–c) Deformation images and (d–f) SEM images of the as-spun P(VDF-TrFE) nanofibers during three various stages of uniaxial tensile test. TXM images of underneath fiber orientation in the insets of (d–f). (g) The engineering stress–strain (S–S) curve. (h–j) The 2D SAXS and (k–m) 2D WAXS patterns. (n) The 1D WAXS patterns. The black arrow represents the tensile direction.

arrangements leading to large strain to failure [36–38] but also induce low tensile strength and elastic modulus [38–40]. The stress increased linearly with strain, implying that stretching and orienting are more dominant during this stage.

The as-spun specimen still experiences the elastic deformation during stage II. The SAXS patterns revealed an oriented arc whose orientation was anisotropic and orthogonal to the tensile direction, attributed to the cavities or microvoids formed during deformation [14]. Such a strong enhancement in the amount of cavities under stretching is responsible for the softening response of as-spun P(VDF-TrFE). No obvious changes of α and β phase diffraction rings were found in the 2D WAXS in Fig. 2(k) and (l), however, the intensity of β phase increased evidently with respect to that of α phase, indicating that stretching promotes a transition from α to β crystalline phase, obtained in Fig. 2(n).

Upon further stretching in the region III of deformation, the stress continuously increased with the increasing strain, suggesting that P(VDF-TrFE) nanofibers were continuously stretched and completely oriented along the straining direction, as demonstrated in both SEM images in Fig. 2(f) and TXM images in the inset. The well-aligned arrangements of surface and internal nanofibers enable the increase of local modulus and local stress as well, thus facilitates the fracture of as-spun membrane. The SAXS in Fig. 2(j) indicates a predominantly orthogonal alignment of large cavities to the tensile axis before leading to fracture of the sample while no significant structure changes were detected in the corresponding 2D WAXS in Fig. 2(m). The as-spun P(VDF-TrFE) exhibits good ductility whose deformation was governed by multiple mechanisms of straightening, stretching, sliding, and orderly arrangement of nanofibers under tensile loading. Such multiple deformation

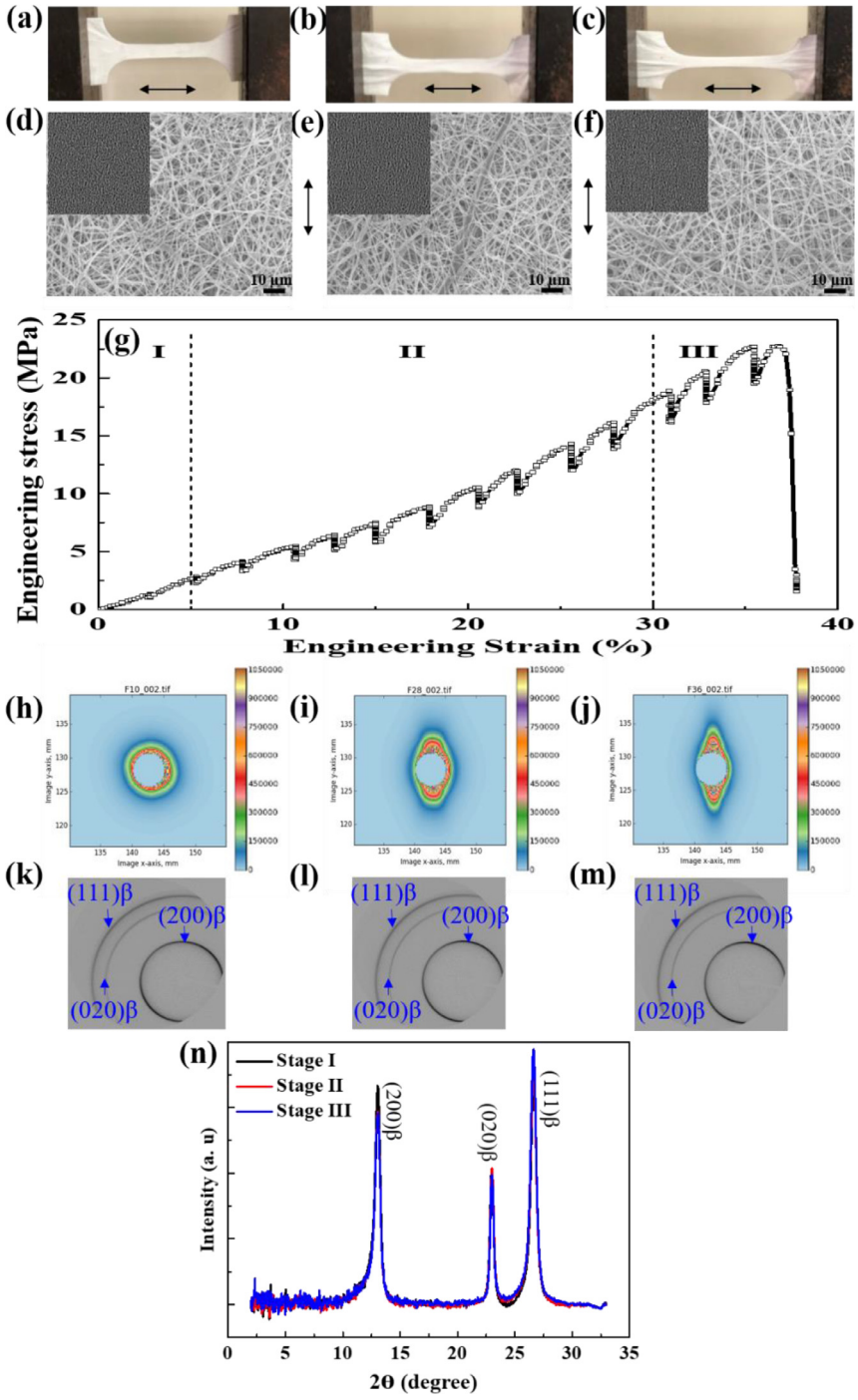

Fig. 3. (a–c) Deformation images and (d–f) SEM images of the annealed P(VDF-TrFE) nanofibers during three various stages of uniaxial tensile test. TXM images of underneath fiber orientation in the insets of (d–f). (g) The engineering stress–strain (S–S) curve. (h–j) The 2D SAXS and (k–m) 2D WAXS patterns. (n) The 1D WAXS patterns. The black arrow represents the tensile direction.

behaviors in the as-spun P(VDF-TrFE) are quite similar to the deformation mechanisms of collagen fibrils in the skin subjected to tensile loading [41].

3.3. Deformation mechanism of annealed P(VDF-TrFE) membrane

Fig. 3 depicts a typical S–S curve for the annealed P(VDF-TrFE) membrane accompanied with the structural features during the stretch-hold operation. The S–S curve shapes of the annealed and as-spun samples were alike, representing the dominant macroscopic elastic deformation. Similar to the as-spun, no neck formation can be observed during stretching deformation in the annealed specimen. Three different stages (I), (II), and (III) correspond to the strain region of 5%, 30%, and before fracture, respectively. Three data points at the strain of 2.5%, 20%, and 32.5% were taken by SEM images to explore the microstructural evolution. The yield strength of the annealed was around 5 MPa which was double greater than the as-spun specimen due to the strong bonding forces between molecular chains in the high content of β crystalline phase after annealing. Moreover, annealing treatment results in an almost three times increase of the Young modulus from 7.4 to 21.4 MPa and a greater elasticity of P(VDF-TrFE) membrane.

The elongation at break of the annealed was found to be 44% which was more than seven times smaller than that of the as-spun specimen. No clear differences of surface morphology of nanofibers were seen in SEM during deformation of the annealed membrane. In contrast to multiple deformation mechanisms in the as-spun, no obvious deformation of the annealed P(VDF-TrFE) was detected. A rise of stress with the

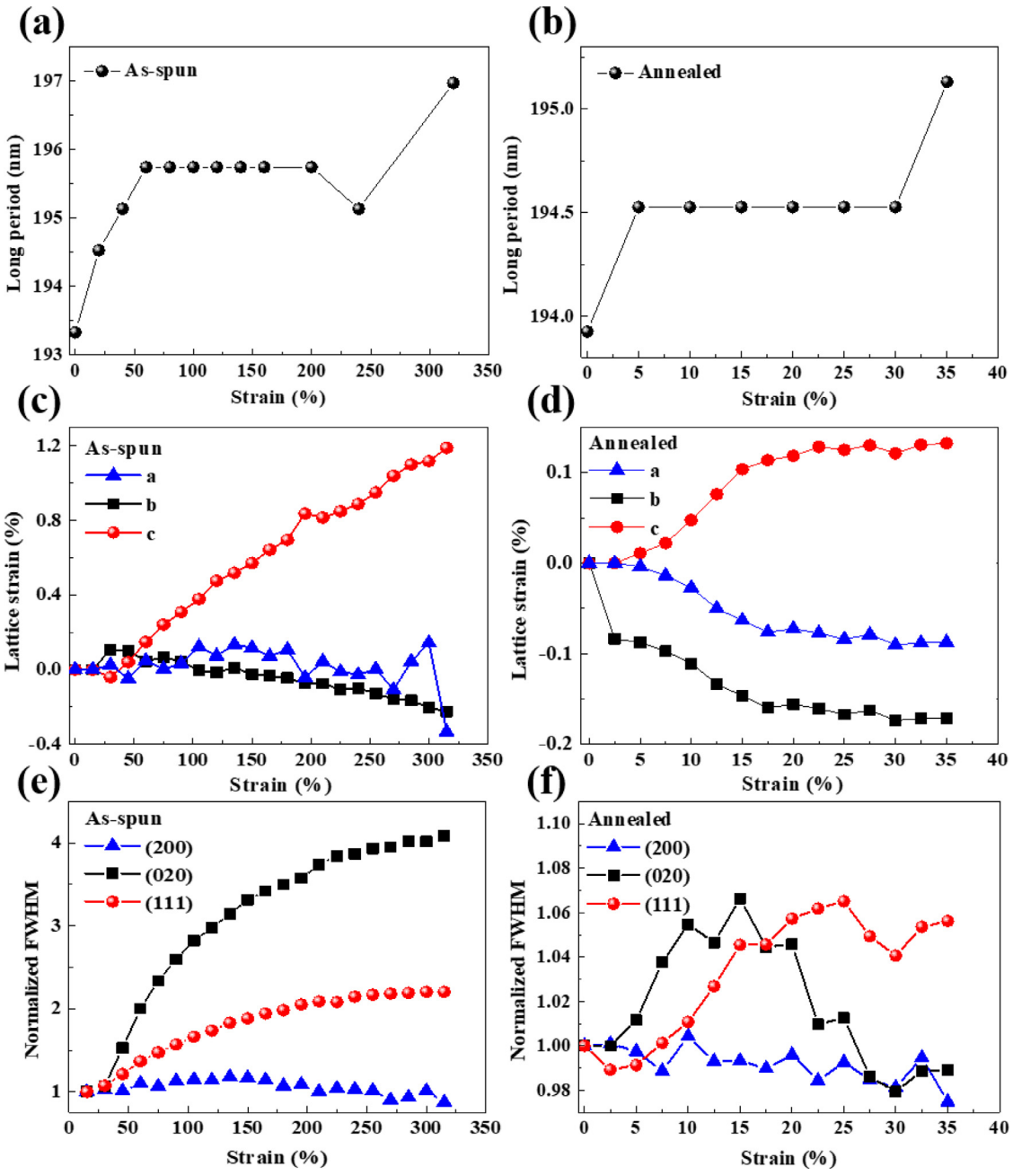

Fig. 4. Long period, unit-cell lattice constants, and FWHM evolution of the as-spun in (a), (c), and (e); and those of the annealed P(VDF-TrFE) nanofibers in (b), (d), and (f), respectively.

increasing strain in the annealed was higher than that in the as-spun, meaning much stress was needed to orient the tightly packing molecule chains induced by polar β crystalline phase and inferring the hard elastic behavior of the annealed sample. In addition, a sharp increase of local modulus and local stress during loading probably hastens the fracture failure, yielding a low elongation to break of the annealed P(VDF-TrFE). Since the defects, cavities, or microvoids were dramatically decreased by annealing treatment, their roles to the deformation in the annealed sample were negligible. There was no appearance of α crystalline phase and the annealed specimen remained the more stable β crystalline phase without crystal structure changes during deformation. Upon straining, the anisotropy pattern in the SAXS represents the orientation of crystalline lamellae orthogonal to the loading direction. In general, the as-spun exhibits a ductile fracture while the annealed membrane reveals a more brittle fracture during uniaxial stretching deformation, attributed to a stiffer behavior of the more β crystalline rather than the more α crystalline phase.

3.4. Evolution of long period and lattice constants

To understand the fiber deformation under stretching at different multi-length scales, we analyzed the long period, unit-cell lattice constants, and full width half maximum (FWHM) versus strain during uniaxial stretching of the as-spun and annealed P(VDF-TrFE). The long periods of as-spun and annealed P(VDF-TrFE) before stretching were around 193 nm. There was a dramatic increase of long period with the increasing strain in the region I of as-spun P(VDF-TrFE) in Fig. 4(a). Such a strong increase of long period in the as-spun specimen completely extends the amorphous chains between crystalline lamella as well results in larger interlamellar spacing of the crystalline lamella planes. No

obvious variation of long period in the region II was obtained, owning to the concurrent straightening, sliding, and orderly orientation of nanofibers besides extending the packed molecular chains. We can observe a similar tendency of long period evolution in the annealed sample in Fig. 4(b), but the increase of long period was four times lower than in the case of as-spun P(VDF-TrFE). Since the annealing treatment did almost tightly pack the tie chains between lamella stacks together, stretching the annealed specimen only slightly results in a very small variation of long period.

We investigated the lattice evolution of *a, b*, and *c* lattice constants to clarify the fiber deformation at lattice level. The β crystalline phase P(VDF-TrFE) is a orthorhombic unit cell with space group *Cm2m* [6,42–45]. Among the three lattice parameters, the lattice constant *c* lengthens much greater in the as-spun than in the annealed sample during straining, as observed in Fig. 4(c) and (d). In Fig. 4(c), the lattice constant *c* dramatically elongates with the increasing strain while the lattice constants *a* and *b* exhibit no significant change during stretching the as-spun P(VDF-TrFE), implying the elongation of the lattice constant c dominantly contributes to the stretching of nanofibers observed in the SEM results. The lattice constant c continues to elongate while the lattice constants a and b slightly shorten in the region III, demonstrating that the nanofibers continue stretching and highly orienting towards the tensile direction which are the major deformation behaviors in this region, in accordance with SEM images. On the other hand, the lattice parameter evolution in Fig. 4(d) expresses a different behavior in which the lattice constant c experiences a prolongation at the similar level as a shrinkage of the lattice constants *a* and *b*. The nanofibers in the annealed specimen are also slightly stretched via the observation in a small increase of long period and expansion of lattice constant c. However, comparing with the remarkable evolution of long period and lattice constant *c* in the as-spun, such a much smaller variation in the annealed specimen leads to the unobivous stretching of nanofibers at the micrometer scale in the SEM images. The dominant deformation behavior of the annealed P(VDF-TrFE) is attributed to the slightly stretched nanofibers coupled with the orientation of crystalline lamellae orthogonal to the straining direction.

The peak-width analysis from WAXS peaks was used to examine the defect evolution during stretching the as-spun and annealed samples in Fig. 4(e) and (f), respectively. A more pronounced broadening of (020) and (111) peak-widths in the as-spun rather than in the annealed specimen implies strong microstructure development of defects, microvoids, or cavities accumulated during deformation of the as-spun P(VDF-TrFE). This result agrees well with our SAXS in which the α and β phase crystallites are oriented along the stretching direction, which is connected by elongated molecular chains along the fibers associated with the accumulated microvoids or cavities across the fibers, resulting in the stretching and well-order arrangements of nanofibers along the straining direction. A trivial variation of FHWH in Fig. 4(f) presents a clear evidence of the negligible presence of microvoids or defects in the β crystalline phase during deformation of the annealed P(VDF-TrFE). The fiber deformation at nanometer and lattice scales helps to explain why no obviously morphological change of the annealed P(VDF-TrFE) was detected by SEM images under straining.

4. Conclusions

Our results demonstrate that annealing is an effective method to trigger a complete transformation from α to β crystalline phase as well as to improve the piezoelectric response in electrospun P(VDF-TrFE) nanofibers. The curvy nanofibers in as-spun P(VDF-TrFE) experience multiple deformation mechanisms of straightening, stretching, sliding, and orderly alignment along the tensile direction while those in annealed P(VDF-TrFE) are slightly extended elastically during straining. The as-spun P(VDF-TrFE) discloses better ductility with a salient elongation of 327% while the annealed sample displays a more brittle fracture with higher strength upon stretching deformation. Our findings provide important mechanical and structural properties for various potential applications of electrospun P(VDF-TrFE) nanofibers in flexible piezoelectric sensing devices.

Declaration of Competing Interest

The authors declare that they have no known competing financial interests or personal relationships that could have appeared to influence the work reported in this paper.

Acknowledgments

The authors are grateful to the support of the Ministry of Science and Technology (MOST) Programs MOST-108-3017-F-009-003, 107-2218-E-007-012, 107-3017-F-009-002, 107-3017-F-007-003, 107-3017-F-009-002, 107-3011-F-002-002, 104-2628-E-009-003-MY3, 106-2811-E-009-032, 106-2218-E-007-019, 106-2514-S-007-004, 106-3011-F-002-002, and 108-2221-E-009-131-MY4. This work was financially supported by the "Center for the Semiconductor Technology Research" from The Featured Areas Research Center Program within the framework of the Higher Education Sprout Project by the Ministry of Education (MOE) in Taiwan. Also supported in part by the MOST, Taiwan, under Grant MOST-108-3017-F-009-003. EWH and TNL are supported by MOST 107-2628-E-009-001-MY3. We greatly appreciate the beam time and help from the NSRRC.

Supplementary material

Supplementary material associated with this article can be found, in the online version, at doi:10.1016/j.mtla.2019.100461.

References

[1] J. Chang, M. Dommer, C. Chang, L. Lin, Piezoelectric nanofibers for energy scavenging applications, Nano Energy 1 (3) (2012) 356–371.
[2] B. Li, F. Zhang, S. Guan, J. Zheng, C. Xu, Wearable piezoelectric device assembled by one-step continuous electrospinning, J. Mater. Chem. C 4 (29) (2016) 6988–6995.
[3] M. Noyori, Y. Neo, H. Mimura, Single-crystalline poly(vinylidene fluoride–trifluoroethylene) nanofiber webs fabricated by electrospinning, Jpn. J. Appl. Phys. 54 (2) (2015) 021601.
[4] D.F.M. Zaccaria, J. Belcari, O. Bocchi, A. Zucchelli, T. Cramer, B. Fraboni, Electret behavior of electrospun PVdF-based polymers, IEEE Conference on Electrical Insulation and Dielectric Phenomena, 2016.
[5] S. Chen, Z. Lou, D. Chen, K. Jiang, G. Shen, Polymer-enhanced highly stretchable conductive fiber strain sensor used for electronic data gloves, Adv. Mater. Technol. 1 (7) (2016) 1600136.
[6] C. Wan, C.R. Bowen, Multiscale-structuring of polyvinylidene fluoride for energy harvesting: the impact of molecular-, micro- and macro-structure, J. Mater. Chem. A 5 (7) (2017) 3091–3128.
[7] Y. Qi, M.C. McAlpine, Nanotechnology-enabled flexible and biocompatible energy harvesting, Energy Environ. Sci. 3 (9) (2010) 1275.
[8] A. Baji, Y.-W. Mai, S.-C. Wong, Effect of fiber size on structural and tensile properties of electrospun polyvinylidene fluoride fibers, Polym. Eng. Sci. 55 (8) (2015) 1812–1817.
[9] Q.M. Zhang, Vivek Bharti, X. Zhao, Giant electrostriction and relaxor ferroelectric, Science 280 (1998) 2101–2104.
[10] Q. Sun, W. Seung, B.J. Kim, S. Seo, S.W. Kim, J.H. Cho, Active matrix electronic skin strain sensor based on piezopotential-powered graphene transistors, Adv. Mater. 27 (22) (2015) 3411–3417.
[11] D. Mao, M.A. Quevedo-Lopez, H. Stiegler, B.E. Gnade, H.N. Alshareef, Optimization of poly(vinylidene fluoride-trifluoroethylene) films as non-volatile memory for flexible electronics, Org. Electron. 11 (5) (2010) 925–932.
[12] Z.H. Liu, C.T. Pan, L.W. Lin, J.C. Huang, Z.Y. Ou, Direct-write PVDF nonwoven fiber fabric energy harvesters via the hollow cylindrical near-field electrospinning process, Smart Mater. Struct. 23 (2) (2014) 025003.
[13] Y. Jiang, L. Gong, X. Hu, Y. Zhao, H. Chen, L. Feng, D. Zhang, Aligned P(VDF-TrFE) nanofibers for enhanced piezoelectric directional strain sensing, Polymers 10 (2018) 364.
[14] H. Guo, Y. Zhang, F. Xue, Z. Cai, Y. Shang, J. Li, Y. Chen, Z. Wu, S. Jiang, In-situ synchrotron SAXS and WAXS investigations on deformation and α–β transformation of uniaxial stretched poly(vinylidene fluoride), CrystEngComm 15 (8) (2013) 1597.
[15] V.B. Ivan Dmitriev, Viktor Lavrentyev, Galina Elyashevich, Structure and deformational behavior of poly(vinylidene fluoride) hard elastic films, Acta Chim. Slov. 54 (2007) 784–791.
[16] J.M.S. Jing Wu, F. Yeh, B.S. Hsiao, B. Chu, In-Situ simultaneous synchrotron small- and wide-angle X-ray scattering measurement of poly(vinylidene fluoride) fibers under deformation, Macromolecules 33 (2000) 1765–1777.

[17] Z. Xu, M. Baniasadi, S. Moreno, J. Cai, M. Naraghi, M. Minary-Jolandan, Evolution of electromechanical and morphological properties of piezoelectric thin films with thermomechanical processing, Polymer (Guildf) 106 (2016) 62–71.
[18] E.W. Huang, Y.H. Hsu, W.T. Chuang, W.C. Ko, C.K. Chang, C.K. Lee, W.C. Chang, T.K. Liao, H.C. Thong, Visible-light modulation on lattice dielectric responses of a piezo-phototronic soft material, Adv. Mater. 27 (47) (2015) 7728–7733.
[19] N.H. Badr-Eddine El Mohajir, Changes in structural and mechanical behaviour of PVDF with processing and thermomechanical treatments. 1. Change in structure, Polymer (Guildf) 42 (2001) 5661–5667.
[20] K.M. Jodie, L. Lutkenhaus, A. Serghei, T.P. Russell, Confinement effects on crystallization and curie transitions of poly(vinylidene fluoride-co-trifluoroethylene), Macromolecules 43 (2010) 3844–3850.
[21] M.H.T. Hattori, H. Ohigashi, The crystallization behaviour and phase diagram of extended-chain crystals of poly(vinylidene fluoride) under high pressure, Polymer (Guildf) 37 (1996) 85–91.
[22] P.P. François Bargain, F.D. Dos Santos, S. Tence-Girault, From solvent-cast to annealed and poled poly(VDF-co-TrFE) films new insights on the defective ferroelectric phase, Polymer (Guildf) 105 (2016) 144–156.
[23] D. Mao, B.E. Gnade, M.A. Quevedo-Lopez, Ferroelectric-Properties-and-Polarization-Switching-Kinetic-of-Poly-Vinylidene-Fluoride-Trifluoroethylene-Copolymer, in: Ferroelectrics—Physical Effects, InTech, Rijeka: Croatia, 2011, pp. 77–101.
[24] M.H. Mohd Wahid, R. Mohd Dahan, S.Z. Sa'ad, A.N. Arshad, M.N. Sarip, M.R. Mahmood, G. Wee Chen, A.M. Wan Haliza, Effect of annealing temperature on the crystallinity, morphology and ferroelectric of polyvinylidenefluoride-trifluoroethylene (PVDF-TrFE) thin film, Adv. Mater. Res. 812 (2013) 60–65.
[25] K. Lau, Y. Liu, H. Chen, R.L. Withers, Effect of annealing temperature on the morphology and piezoresponse characterisation of poly(vinylidene fluoride-trifluoroethylene) films via scanning probe microscopy, Adv. Condens. Matter Phys. 2013 (2013) 1–5.
[26] M. Baniasadi, Z. Xu, J. Cai, S. Daryadel, M. Quevedo-Lopez, M. Naraghi, M. Minary, Correlation of annealing temperature, morphology, and electro-mechanical properties of electrospun piezoelectric nanofibers, Polymer 127 (2017) 192–202.
[27] N. Hussain, M.-H. Zhang, Q. Zhang, Z. Zhou, X. Xu, M. Murtaza, R. Zhang, H. Wei, G. Ou, D. Wang, K. Wang, J.-F. Li, H. Wu, Large piezoelectric strain in sub-10 nanometer twodimensional polyvinylidene fluoride nanoflakes, ACS Nano 13 (2019) 4496–4506.
[28] E. Jin Ko, S. Jae Jeon, Y. Woon Han, S. Yeong Jeong, C. Yun Kang, T. Hyun Sung, K. Won Seong, D. Moon, Synthesis and characterization of nanofiber-type hydrophobic organic materials as electrodes for improved performance of PVDF-based piezoelectric nanogenerators, Nano Energy 58 (2019) 11–22.
[29] S.S. Kwak, H.-J. Yoon, S.-W. Kim, Textile-based triboelectric nanogenerators for self-powered wearable electronics, Adv. Funct. Mater. 29 (2) (2019) 1804533.
[30] T.-N. Lam, W.-J. Huang, C.-C. Wang, W.-T. Chuang, Y.-W. Su, E.W. Huang, Micro-layer and lattice structure effects on impedance of titanium oxide phthalocyanine, Adv. Eng. Mater. 20 (7) (2018) 1701140.
[31] C.C. Wang, Y.F. Song, S.R. Song, Q. Ji, C.C. Chiang, Q. Meng, H. Li, K. Hsiao, Y.C. Lu, B.Y. Shew, T. Huang, R.R. Reisz, Evolution and function of dinosaur teeth at ultramicrostructural level revealed using synchrotron transmission X-ray microscopy, Sci. Rep. 5 (2015) 15202.
[32] P.-I. Tsai, T.-N. Lam, M.-H. Wu, K.-Y. Tseng, Y.-W. Chang, J.-S. Sun, Y.-Y. Li, M.-H. Lee, S.-Y. Chen, C.-K. Chang, C.-J. Su, C.-H. Lin, C.-Y. Chiang, C.-S. Ku, N.-T. Tsou, S.-J. Shih, C.-C. Wang, E.W. Huang, Multi-scale mapping for collagen-regulated mineralization in bone remodeling of additive manufacturing porous implants, Mater. Chem. Phys. 230 (2019) 83–92.
[33] C.Y. Liu, X. Li, W.Y. Chen, L.C. Chang, Y.F. Chen, H.L. Chen, Y.S. Sun, H.Y. Lai, E.W. Huang, PEGylation site-dependent structural heterogeneity study of monoPEGylated human parathyroid hormone fragment hPTH(1-34), Langmuir 30 (38) (2014) 11421–11427.
[34] S. Kaur, A. Kumar, A.L. Sharma, D.P. Singh, Influence of annealing on dielectric and polarization behavior of PVDF thick films, J. Mater. Sci.: Mater. Electron. 28 (12) (2017) 8391–8396.
[35] Y. Jiang, S. Shiono, H. Hamada, T. Fujita, D. Zhang, K. Maenaka, Reactive ion etching of poly(vinylidene fluoride-trifluoroethylene) copolymer for flexible piezoelectric devices, Chin. Sci. Bull. 58 (17) (2013) 2091–2094.
[36] P. Isaksson, An implicit stress gradient plasticity model for describing mechanical behavior of planar fiber networks on a macroscopic scale, Eng. Fract. Mech. 77 (8) (2010) 1240–1252.
[37] S. Buell, G.C. Rutledge, K.J. Vliet, Predicting polymer nanofiber interactions via molecular simulations, ACS Appl. Mater Interfaces 2 (4) (2010) 1164–1172.
[38] U. Stachewicz, I. Peker, W. Tu, A.H. Barber, Stress delocalization in crack tolerant electrospun nanofiber networks, ACS Appl. Mater Interfaces 3 (6) (2011) 1991–1996.
[39] X.-F. Wu, Y.A. Dzenis, Adhesive contact in filaments, J. Phys. D Appl. Phys. 40 (14) (2007) 4276–4280.
[40] E.M. Huisman, C. Heussinger, C. Storm, G.T. Barkema, Semiflexible filamentous composites, Phys. Rev. Lett. 105 (11) (2010) 118101.
[41] W. Yang, V.R. Sherman, B. Gludovatz, E. Schaible, P. Stewart, R.O. Ritchie, M.A. Meyers, On the tear resistance of skin, Nat. Commun. 6 (2015) 6649.
[42] A.J. Lovinger, Conformational defects and associated molecular motions in crystalline poly(vinylidene fluoride), J. Appl. Phys. 52 (10) (1981) 5934–5938.
[43] J.B. Lando, H.G. Olf, A. Peterlin, Nuclear magnetic resonance and x-ray determination of the structure of poly(vinylidene fluoride)†, J. Polym. Sci. Part A-1 4 (1966) 941–951.
[44] P. Scardi, L. Rebuffi, M. Abdellatief, A. Flor, A. Leonardi, Debye–Waller coefficient of heavily deformed nanocrystalline iron this article will form part of a virtual special issue of the journal, presenting some highlights of the 13th biennial conference on high-resolution X-ray diffraction and imaging (XTOP2016), J. Appl. Crystallogr. 50 (2) (2017) 508–518.
[45] M. Leoni, J. Martinez-Garcia, P. Scardi, Dislocation effects in powder diffraction, J. Appl. Crystallogr. 40 (4) (2007) 719–724.